Journal of Casting & Materials Engineering Vol. 8 No. 1 (2024) 1–10
https://doi.org/10.7494/jcme.2024.8.1.1

Solidification Process Modeling of Equiaxed Investment Castings with Transient Nonuniform Boundary Condition Definition

Weston Olson[ab*], Michael Stemmler[b], Erik Fernandez[a], Jayanta Kapat[a]

[a] University of Central Florida, Center for Advanced Turbomachinery and Energy Research, 4000 Central Florida Blvd, Orlando, FL 32816
[b] Siemens Energy, Gas Services Central Large Gas Turbine Engineering, 11842 Corporate Blvd, Orlando, FL 32817
**e-mail:* weston.olson@siemens-energy.com

Received: 22 November 2023/ Accepted: 22 February 2024/Published online: 30 March 2024.
This article is published with open access at the AGH University of Science and Technology Journals.

Abstract

The equiaxed investment casting process is a multi-physics problem which requires knowledge from engineers who have expertise in materials, metallurgy, fluid dynamics, thermodynamics, and heat transfer. Process modeling is a tool used by foundries to help predict casting defects such as shrinkage porosity, hot tears, and poor grain structure. The reliability of these predictions is strongly dependent on the accuracy of the thermal boundary conditions set in the model. In this work, a SGT5-2000E Vane 4 cast in Rene 80 nickel-based superalloy was modeled, using the FEA simulation package ProCAST, with two different methodologies. One methodology had very little effort invested into defining the thermal domain. The other methodology involved a thorough consideration of all heat transfer mechanisms acting on the mold. An extensive literature search was performed to define a unique natural convection heat transfer coefficient for each set of surfaces on the mold. The transient boundary layer development was also captured in the definition of the heat conditions. The shrinkage porosity predictions of the models were compared to real-world x-ray data and the transient nonuniform methodology predictions were much more representative than the low fidelity heat transfer methodology predictions. The low fidelity heat transfer model did predict some shrinkage, but not where it appeared in reality. The process modeler will be misdirected by the model results when deriving a solution to the casting process if the real-world physics are not appropriately accounted for in the model. This will be very counterproductive when the foundry is using the model to reduce developmental trials by running trials in model space. References and derived parameters are provided for material properties, emissivity of shell and insulation wraps, and external mold spatially varying heat transfer coefficients.

Keywords:

solidification process modeling, casting simulation, nickel-based superalloy, equiaxed investment casting, large gas turbine hardware, transient nonuniform heat transfer, natural convection, ProCAST

1. INTRODUCTION

Solidification process modeling is practiced by all foundries who manufacture large gas turbine hardware. The material properties, emissivity, heat transfer coefficients, etc. and methodology used by the foundries is considered highly proprietary and strictly confidential. To the best knowledge of the authors, there are no previous publications with respect to equiaxed investment castings of large gas turbine hardware. Zhang et al. [1] performed equiaxed investment casting experiments on a single cored airfoil to derive an interface heat transfer coefficient (IHTC) relationship between the alloy and the shell. The alloy used in his study was aluminum alloy A355 and the ProCAST simulation was validated by experimental results. Szeliga et al. [2] conducted an experiment to determine the interface heat transfer coefficient between IN713C and the ceramic shell mold. The geometry casted was a flat plate oriented horizontally. The findings of the study concluded that the IHTC had a value of 7962 $W/(m^2 \cdot K)$ at the liquidus temperature sharply decreased during cooling and close to the solidus temperature an increase in magnitude was observed. The secondary peak near the solidus temperature was assumed to be due to mixed oxide scaling at the interface. Sahai and Overfelt [3] investigated the IHTC for various geometries with IN718. The conclusions of their investigation showed that for the cylindrical casting the IHTC varied from 200 to 100 $W/(m^2 \cdot K)$ and for the flat plate it varied from 5000 to 100 $W/(m^2 \cdot K)$. Yang et al. [4] used ProCAST to explore process optimization of an investment cast low pressure turbine blade. The investigation included three different wax pattern configurations and orientations. The blade geometry was hypothetical, and the alloy used was an intermetallic titanium aluminide alloy. The results consisted of a matrix of casting parameters and their corresponding volumes of porosity. Lenda et al. [5] performed solidification process modeling in ProCAST on a simple rectangular casting with the nickel-based superalloy Hastelloy G30. The porosity predictions of the ProCAST model were validated by optical

microscopy which revealed pores in the center of the casting. Miao et al. [6] conducted numerical simulation of an investment casting process for a simple cone like casting with AlSil1 alloy and reported the predicted amount of porosity using ProCAST. Liao et al. [7] investigated the solidification process of a titanium alloy gearbox and validated the ProCAST simulation results to a real-world casting. There are several other studies which use solidification process modeling to validate real-world casting quality and/or optimize the casting process in model space [8–13]. Most of the previous work in the literature consists of applications on simple geometries and no detailed descriptions of the external mold heat conditions are provided. There are also very few studies of solidification process modeling with nickel-base superalloys.

In this work, an actual casting process from a real foundry, Siemens Energy's foundry, was modeled on a large gas turbine hot gas path component, SGT5-2000E Vane 4, and the results were validated against real-world x-ray data. The external mold heat condition modeling methodology is explained in detail for both the low fidelity and the transient nonuniform models. From the fundamental understanding of natural convection, and the extensive studies available in the literature, one knows that the free convection heat transfer coefficient depends on several different factors. These factors include, but are not limited to, the surface temperature or surface heat flux, surface roughness, surface permeability, surface orientation, surface curvature, surface vertical height, etc. From this fundamental knowledge one knows that differently sized, oriented, and shaped surfaces of the mold will have unique external heat transfer coefficients. Hence, the free convective mechanism for investment casting processes will be nonuniform in nature. To the knowledge of the authors, the only transient studies available in the literature are for the cases where the initial temperature difference, between ambient air and heated surface, is zero. For the application of investment castings, this initial condition is not applicable. Assumptions on the transient nature of the boundary layer will have to be made in order to use the existing data in the literature.

Hellums and Churchill [14] provided the first complete solution for transient free convection for any geometry and the results consisted of velocity, temperature, and heat transfer coefficient as a function of time. The application for the study was an isothermal vertical plate. Goldstein and Briggs [15] investigated the penetration distance for a transient developing boundary layer. The study resulted in several correlations for multiple scenarios such as step in surface flux and step change in surface temperature. Salmanpour and Zonouz [16] studied the effect of curvature on steady state heat transfer coefficient numerically. The results concluded that the heat transfer decreases for concave shapes and increases for convex shapes. Bhowmik et al. [17] performed experiments on transient natural convection over a horizontal cylinder. The results of the experiments showed that transient heat transfer strongly depended on position along the cylinder. The stagnation point, or the lowest point of the cylinder, had the least transient heat transfer. Transient heat transfer data was provided as a function of the Fourier number. Eckert and Jackson [18] derived Nusselt number correlation for a turbulent boundary layer over a constant vertical isothermal surface. Moran and Lloyd [19] investigated the dependency of heat transfer on orientation with respect to gravity. They concluded that the Grashof number can be scaled by cosine of the angle the surface makes with the gravity vector. Vliet and Ross [20] studied the turbulent flow along vertically inclined upward and downward facing plates. They found that for upward facing surfaces the Nusselt number was independent of angle and for downward facing surfaces the Grashof number should be scaled by cosine square of the angle. Hrycak and Sandman [21] studied the heat transfer for a downward facing horizontal surface and provided a correlation for such an orientation. Fishenden and Saunders [22] investigated, and derived a correlation, for an upward facing isothermal surface. Bandyopadhyay et al. [23] studied the transient effects of horizontal isothermal flat plates. The data presented in their work was the Nusselt number as a function of the Fourier number. They also provided the time to reach steady state as a function of Rayleigh number.

Almost all of the correlations provided in the literature are for constant surface or constant heat flux applications but this scenario is not applicable to investment casting. Therefore, one should know that when using these correlations assumptions and approximations must be made for their theoretical application to investment castings. The major deviations from the available studies in the literature and physical phenomena of investment casting transient natural convection heat transfer is the initial condition and the surface boundary condition, with the initial condition being that the heated surface and the ambient temperature are initially the same. The surface boundary condition is a constant surface temperature or constant heat flux.

Understanding the entire heat transfer domain and capturing the various mechanisms in the model setup is imperative for reliable predictions. A summary of the various heat transfer mechanisms at each event in the casting sequence will be presented. The casting setup modeled will be described which includes the wax pattern assembly, gating configuration, insulation wrapping scheme, materials, and the surfaces selected for nonuniform heat condition definition. The natural convection investigations previously referenced will then be used to derive the transient heat transfer coefficients for each spatially varying surface condition. References for the emissivity used for shell and insulation wrap surfaces will also be provided when describing the transient spatially varying heat condition derivation. The definition of the thermal conditions for the low fidelity model will be explained and key differences between both methodologies will be highlighted. The results consist of evaluating the fraction solid and the total shrinkage porosity criteria for both the low fidelity and the transient nonuniform models. Explanation for methodology on evaluating the fraction solid result will also be provided. The explanation will place the emphasis on the law of conservation of mass. The results of both models are compared with real-world x-ray data. The summary of the study, a recommendation for best practices in modeling, and areas which require further investigation are used to conclude this paper.

2. HEAT TRANSFER MECHANISMS FOR THE INVESTMENT CASTING PROCESS

Understanding the various heat transfer mechanisms at each event of the casting process is essential in being able to set-up the solidification process model correctly. The investment casting process is a highly transient multi-mode heat transfer process. At each event in the casting process there are different mechanisms of different modes acting on the mold and alloy. Table 1 gives a general outline for a typical investment casting process. Most foundries have some variations between their general casting process and what is outlined in Table 1. The time duration of each of these events will also vary across foundries and across castings within the foundry. The specific sequence of events and their corresponding times is considered proprietary information to the foundry. The casting process modeled in this study consists of the events outlined in Table 1.

Table 1
Typical sequence of events for general investment casting process

#	Event
1	Mold transfer from pre-heat oven to furnace
2	Furnace pump down
3	Furnace vacuum hold
4	Mold fill
5	Furnace vacuum hold
6	Furnace vacuum break
7	Mold transfer from furnace to cooling zone

For all the events there will be internal and external heat transfer mechanisms acting on the mold. The internal mechanisms consist of transient conduction through the shell and insulation wraps along with a thermal contact resistance between contacting surfaces of the insulation wraps. The transient conduction through the mold is defined by the thermal diffusivity, which is a function of the material properties. Specifically, the thermal conductivity, density, and specific heat. The thermal diffusivity plays a very key role in the transient internal heat transfer as it determines how quickly, or slowly, the mold gains, or losses, heat. These internal heat transfer mechanisms will act on the mold during all events of the casting process.

The other internal mechanisms of the mold consist of heat exchange with the alloy. The internal mechanisms of heat transfer between mold and alloy will vary between the mold filling event and the post filling events. For the mold filling event the internal mechanisms consist of radiation, forced convection (for moving fluid), and conduction (for stationary fluid). During the post pour events the mechanism will be conduction until the gap between shell and alloy begins to form. The gap formation is a result of the alloy densification during solidification. According to the conservation of mass, the only way for a liquid to densify into a solid is for there to be a reduction in volume. Hence, the alloy shrinks, and its total volume is reduced. Once the gap between the shell and alloy begins to form, the conduction mechanism converts to a thermal contact resistance mechanism.

This thermal contact resistance between the shell and the alloy is commonly referred to as the interface heat transfer coefficient (IHTC). The interface heat transfer coefficient can be a combination of radiative with convective, or conductive, heat transfer modes. During the vacuum hold the interface heat transfer coefficient will only depend on radiation. The interface heat transfer coefficient strongly depends on the gap width which drives the view factor value for the radiation within the gap. Once the vacuum hold is broken, and air is introduced into the domain, the interface heat transfer coefficient becomes dependent on the total conductance of radiative and convective heat transfer. The convective heat transfer mechanism will be that of natural convection within an enclosure. The reader is referred to work by Yang [24] for details on natural convection within enclosures. The heat transfer coefficient associated with this type of convective mechanism is also dependent on the gap width between the shell and the alloy. Once thermal equilibrium is reached between the gap surfaces and their corresponding boundary layers, the buoyancy forces will diminish. When the air is stagnant within the gap the total conductance for the interface heat transfer coefficient will be a combination of radiation and conduction. The conduction mechanism is also a function of the gap width.

For cored castings there is no gap formation between the alloy and the ceramic core. Since the alloy is compressing onto the core, the heat transfer mechanism between alloy and core is quite different than that of alloy and shell. To the best of the authors knowledge, there are no known studies on the heat exchange between alloy and core during solidification. It is assumed to be a conductive mechanism with a dynamic temperature gradient which is dependent on the rate of contraction of the alloy.

The external mechanisms of the mold exchanging heat with the surroundings will be unique for each event of the casting process. For the mold transfer from pre-heat oven to furnace event the radiative mechanism can be extremely complex. The mold is in motion therefore its view factor, with the surroundings, is constantly changing. Each infinitesimal surface of the mold will have a unique view factor with several other surfaces, each with a different emissivity, a different temperature, and a different surface area. The convective mechanism is also very complex for this event. The mold surfaces are much hotter than the ambient air so there will be natural convection due to the buoyancy forces. The buoyancy forces are the bulk motion of the air due to the density difference near the surface, which is driven by the temperature difference. Depending on the velocity, and overall size, of the mold during transfer, forced convection can also be significant. Therefore, the convective mechanism could consist of mixed forced and free convection heat transfer.

Once the mold is in the furnace and the door is shut, the radiative heat exchange of the mold is with the internal furnace surfaces and with the surfaces of the mold itself. During the pump down stage, air is being pulled out of the furnace and the pressure is decreasing until it reaches a vacuum state. According to the ideal gas law, density is directly proportional to pressure. Therefore, the buoyancy forces which are driven by the density gradient will be decreasing with the pressure during the pump down event. Since it is the buoyancy forces

which drive the bulk motion, the convective mechanism will decrease to a value of zero during the pump down event.

While the mold is filling with the liquid alloy the only external mechanism between the mold and the surroundings is the radiation with the internal furnace surfaces. The radiation will be driven by the view factors between mold surfaces and furnace surfaces, the emissivity, temperature, and surface area of these corresponding surfaces. The external mold surfaces will also be exchanging radiation with other mold surfaces which have a line of site, and a temperature difference, between one another.

During the vacuum break, event air is re-introduced into the domain. Initially there will be a surge of air which is pulled in through the vents of the furnace. Depending on the location of these vents with respect to the mold, this could result in forced convection on the mold. With the furnace being re-pressurized a density gradient at the external mold surfaces will form due to the temperature difference between the surface and the ambient air. This density gradient will drive a transient buoyancy force. Hence, natural convection is expected to be dependent on the transient pressure within the furnace.

For the mold transfer from furnace to cooling zone the radiative mechanism will be the same as the initial mold transfer event. The convective mechanism will also be the same, where it could be a combination of forced and free convection. The key distinction between this event and the initial is that the temperature gradient normal to the surface is driven by the energy released by the alloy during solidification. The radiation exchange may also be with different surfaces at different temperatures and emissivity than the initial event.

Understanding the variations in heat transfer mechanisms for each event and knowing how to account for them in the model setup is critical for obtaining reliable prediction results. Assumptions and approximations must be made to appropriately capture the real-world physics in the model. It would be very unpractical to include the entire surroundings domain during mold transfer into the solidification model. It is left to the process modeler to determine which assumptions and approximations are appropriate and how to apply them accordingly. Regardless, all events which influence the mold temperature should be captured in the model. The temperature gradient within the mold, at the moment that heat exchange with the alloy occurs, is a key influencer on the resulting internal temperature gradient of the alloy. This internal temperature gradient of the alloy greatly influences the quality of the casting and whether it will have an acceptable level of shrinkage or not. The process modelers capability to capture the real-world physics by applying the appropriate assumptions and approximations is considered a necessary skill in setting up the solidification model for reliable predictions.

3. CASTING SETUP

The casting setup for SGT5-2000E Vane 4 is now described. To adhere to intellectual property restrictions of the foundry, some of the process parameters will not be specified. The wax pattern assembly is a one-by-one, horizontally oriented casting which is gated from the suction-side mate faces (Fig. 1).

The insulation wrapping scheme consisted of a three-step airfoil wrap with a single layer over the gating system (Fig. 2). The green insulation wrap represents one layer, the pink wrap represents two layers, and the cyan wrap represents three layers.

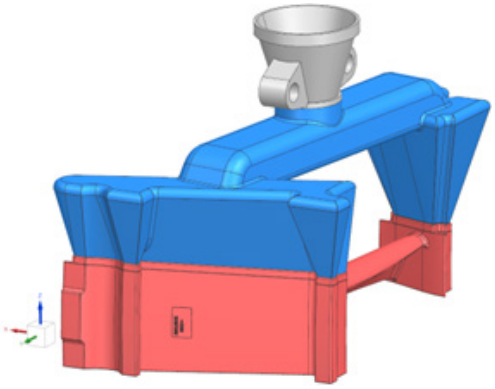

Fig. 1. Wax pattern assembly

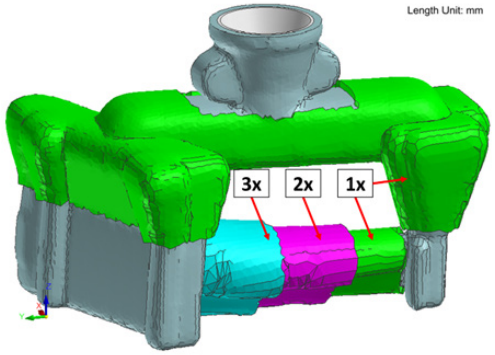

Fig. 2. Mold insulation wrapping scheme

The material properties of shell, insulation wraps, and alloy were taken from the ProCAST public database as ceramic refractory mullite, wrap kaowool, and Ni Rene 80, respectively. As summarized in the introduction, natural convection depends on several variables. The variables of interest for this application are the surface size, orientation, curvature, and vertical height. These are defined as the variables of interest since surface roughness and permeability are assumed to be relatively constant across all external surfaces of the mold. The surface temperature is initially constant across the entire external surfaces of the mold after soaking in the pre-heat oven for several hours.

The nonuniform heat transfer coefficient surfaces selected to have a unique heat condition are the convex (CV) and concave (CC) sides of the airfoil, OD and ID platforms (ODPF and IDPF), OD and ID gates (ODGate and IDGate), OD and ID pressure side mate-faces (ODMF and IDMF), and the horizontal top sides of the OD and ID gates (ODHz and IDHz) (Fig. 3). The nonuniform natural convection characteristics for the surfaces previously mentioned are as follows: surface curvature for CV and CC; flat vertical for OD and ID platforms; flat angled for OD and ID gates; horizontal downward facing for OD and ID pressure side mate-faces; and horizontal upward facing for horizontal top sides of OD and ID gates.

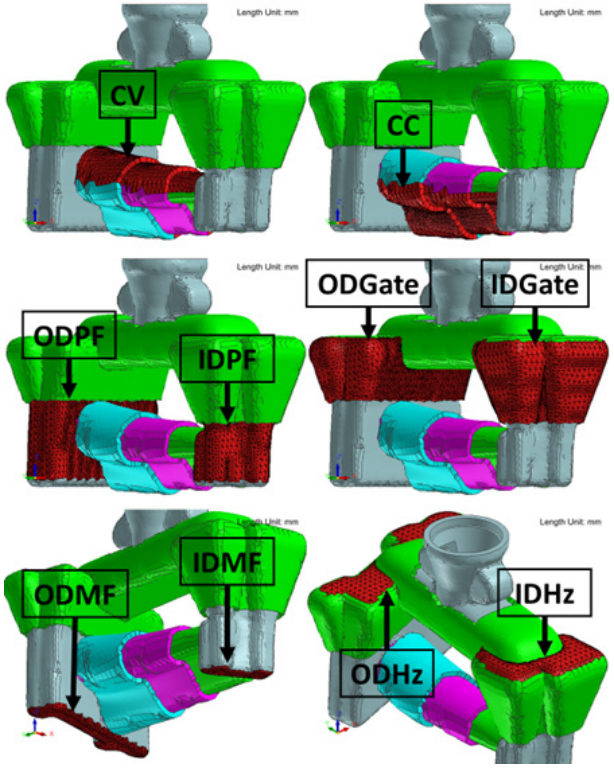

Fig. 3. Nonuniform heat condition surfaces

4. TRANSIENT NONUNIFORM HEAT CONDITION DERIVATION

There was a unique thermal condition for each region of the mold, the surfaces highlighted in Figure 3. The heat condition in ProCAST consists of a region and a corresponding boundary condition. The parameters used to define the boundary conditions in this study were the heat transfer coefficient (termed as film coefficient in ProCAST) as a function of temperature and time, the emissivity as a function of temperature, the ambient temperature as a constant, with the view factor option enabled. The heat transfer coefficient was defined as a function of temperature because all the correlations found in the literature are a function of the Grashof number, Equation (1).

$$Gr_L = \frac{g\beta(T_s - T_\infty)L^3}{\nu^2} \tag{1}$$

where:

g – acceleration of gravity [m/s^2],
β – coefficient of thermal expansion [K^{-1}],
T_s – surface temperature [K],
T_∞ – ambient temperature [K],
L – characteristic length [m],
ν – kinematic viscosity [m^2/s].

Defining the heat transfer coefficient as a function of time gives the capability to capture the transient effects associated with boundary layer development, furnace pump down, and furnace vacuum break events. The emissivity of refractory mullite was defined as a function of temperature and values were obtained from Bauer et al. [25]. Temperature dependent emissivity of kaowool was provided by Jones et al. [26]. Before using the data provided in the literature to derive the nonuniform transient heat transfer coefficients, assumptions must be made so the data may be applicable. Therefore, these assumptions will classify the following derived relationships as approximations and not exact functions. The assumptions, and their reasonings, are as follows:

- All spatially varying heat transfer coefficient surfaces have a negligible temperature variance. They are all insulating materials, highly resistant to temperature change, with the same initial temperature. This allows for application of isothermal correlations provided in the literature.
- Transient heat transfer has an increasing linear relationship until steady state is reached and over/under shoots in boundary layer development are negligible. Without any previous investigations there is no better way to qualify the transient behavior for the initial condition in this application.
- Forced convection during mold transfer is negligible. The mold velocity is relatively low.
- Location of vents in furnace relative to mold will have negligible effect on forced convection during vacuum break.
- Heat transfer coefficient linearly decreases and increases proportionally with pressure for pump down and vacuum break, respectively. The buoyancy forces are driven by the density gradient on the external mold surface, which is dependent on the pressure within the furnace.
- If steady state heat transfer is reached before pump down event, the heat transfer coefficient will decrease linearly from the steady state value to a value of zero. For all transient studies referenced in this investigation there was heat generated in the system. For this application no heat is generated before the mold filling event. Therefore, once steady state values are reached the mold surfaces will further cool and buoyancy forces will decrease.
- Heat flux from mold is constant during solidification.

Results from the investigation by [16] were used to derive a heat transfer coefficient relationship for concave and convex surfaces of the airfoil. The data provided by this study consists of heat transfer coefficients as a function of vertical height and curvature angle for both concave and convex surfaces all with the same temperature difference between wall and ambient. The temperature difference and geometric data was used to calculate the Rayleigh number. The Rayleigh number is the product of the Grashof number and the Prandtl number. This Rayleigh number was used as the reference number to derive a Rayleigh ratio with the Rayleigh numbers associated with the geometry and temperature range of interest. This Rayleigh ratio was used as a scaling factor to scale the Nusselt number provided from [16] at each temperature of interest. The heat transfer coefficient was then calculated by this scaled Nusselt number. Now an approximation, based on experimental data, is available for the heat transfer dependency on temperature for the airfoil surfaces. This dependency is defined by the

dimensionless heat transfer group, Equation (2), as a function of the temperature difference between surface and ambient.

$$h^* = \frac{h}{k}\left(\frac{\nu^2 x}{g\beta(T_s - T_\infty)}\right)^{1/4} \tag{2}$$

where:

h – heat transfer coefficient W/(m² · K),
k – thermal conductivity W/(m · K),
ν – kinematic viscosity [m²/s],
x – vertical position along wall [m],
g – acceleration of gravity [m/s²],
β – coefficient of thermal expansion [K⁻¹],
T_s – surface temperature [K],
T_∞ – ambient temperature [K].

The transient dependency approximation was made based off data provided by [17]. The data had steady state heat transfer at a Fourier number of approximately 40. The thermal diffusivity and characteristic length of the system of interest were used with the Fourier number to solve for the time, Equation (3).

$$t = \frac{FoL^2}{\alpha} \tag{3}$$

where:

t – time [s],
Fo – dimensionless Fourier number [–],
L – characteristic length [m],
α – thermal diffusivity [m²/s].

The authors of [17] state that for any given heat flux, the temperature increased sharply with time. With this statement it is assumed that the temperature of the horizontal cylinder did not vary with time shortly after the heat flux was initiated. The experimental setup in [17] as well as many other studies in the literature differ from the investment casting process in this way. For equiaxed investment castings the mold temperatures will always be in a transient state. Therefore, the time calculated to reach steady state was an average of the steady state Fourier number parameters at preheat temperature to the steady state Fourier number parameters at a temperature halfway to room temperature. This approximation was driven by the fact that the Fourier number is a function of the thermal diffusivity, and the thermal diffusivity is a function of surface temperature.

The characteristic length through which conduction acts was taken as the thickness of a single layer of insulation. This was done because there is an intermediate mechanism at the interfaces of the contacting surfaces of insulation layers. This intermediate mechanism is the thermal contact resistance. Therefore, the same transient time dependency for both convex and concave surface of the airfoil was used. The transient relationship will be defined as the heat transfer coefficient factor as a function of the dimensionless time, Equation (4), for the time interval between pre-heat oven to pump down. The heat transfer coefficient factor is multiplied by the temperature dependent relationship. This factor will essentially represent the development of the transient boundary layer.

$$t^* = \frac{t}{t_{(pre-pump)}} \tag{4}$$

where $t_{pre\text{-}pump}$ is pre-heat to pump down time [s].

According to the assumptions stated at the beginning of this section, the heat transfer coefficient will have linear relationships during the pump down and vacuum break events. The vacuum break duration is less than the time required for the boundary layer to reach steady state. This behavior will be illustrated in one of the following plots.

The average Nusselt number correlation, Equation (5), for turbulent flow along a vertical flat plate provided by [18] was used to define the temperature dependent heat transfer coefficient for OD and ID platform surfaces.

$$Nu_{ave} = 0.0834 Ra^{1/3} \tag{5}$$

where *Ra* is dimensionless Rayleigh number.

Correlations derived by [15] were rearranged to solve for the time for the boundary layer to completely penetrate the entire length of the platform surfaces, Equation (6).

$$t_{penetrate} = \sqrt{\frac{x_p}{0.00364 g\beta(T_s - T_\infty)}} \tag{6}$$

where x_p is penetration distance (vertical length) [m].

Findings by [20] were used to define the heat transfer coefficients for the OD and ID gating surfaces. These surfaces are angled with respect to the gravity vector with heated surfaces facing downward. Therefore, Equation (5) was modified to account for the angle of these surfaces, Equation (7). The application of the cosine squared term is valid for downward facing surfaces angled up to 80 degrees with the gravity vector.

$$Nu_{ave} = 0.0834(\cos^2\gamma Gr_L Pr)^{1/3} \tag{7}$$

where:

γ – angle between surface and gravity vector [°],
Pr – dimensionless Prandtl number.

The gravity term in Equation (6) was modified to account for the angle which the surface makes with the gravity vector, Equation (8).

$$t_{penetrate} = \sqrt{\frac{x_p}{0.00364\cos^2 g\beta(T_s - T_\infty)}} \tag{8}$$

The Nusselt number correlation derived by [21] was used for the downward facing horizontal surfaces of the pressure side mate-faces, Equation (9).

$$Nu = 0.0017 Ra^{0.596} \tag{9}$$

The transient relationship was derived from data presented by [23]. The data consisted of the steady state Fourier number as a function of the Rayleigh number. A trendline was created between the data points provided by [23] and this equation was used to populate the Fourier number across the Rayleigh numbers of interest. The time was solved by using Equation (3) where the characteristic length was the ratio of surface area to perimeter and the thermal diffusivity was that of refractory mullite. Since the Fourier number was presented as a function of the Rayleigh number the resulting transient relationships vary for the OD and ID mate-faces due to the large difference in surface size.

The correlation derived by [22] for the Nusselt number of an isothermal upward facing surface was used to define the heat transfer coefficient for the OD and ID horizontal gating surfaces, Equation (10).

$$Nu = 0.54Ra^{1/4} \tag{10}$$

The same procedure was used to derive the transient definition as was for the mate-face surfaces. The change in surface size, thermal diffusivity, and length through which conduction occurs have all significantly changed from the mate-face surfaces. Some considerable differences, in transient derivations, between both sets of horizontal surfaces will result from these variations.

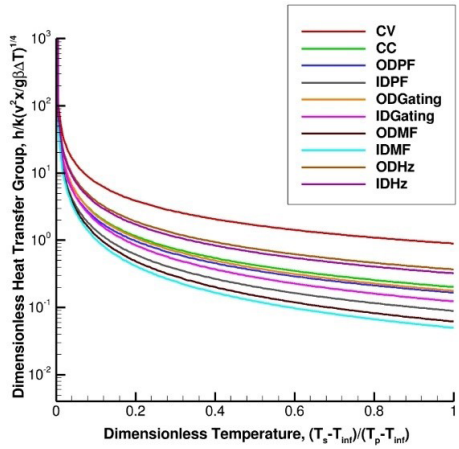

Fig. 4. Temperature dependent heat transfer for spatially varying heat transfer coefficient surfaces

Figure 4 illustrates the dimensionless heat transfer group as a function of dimensionless temperature, Equation (11), for all spatially varying heat transfer coefficient surfaces.

$$\theta^* = \frac{(T_s - T_\infty)}{(T_p - T_\infty)} \tag{11}$$

where T_p is pre-heat temperature [K].

The plot illustrates that each surface will indeed have a unique heat transfer coefficient. Figure 5 illustrates the heat transfer coefficient factor as a function of dimensionless time for all spatially varying heat transfer coefficient surfaces.

Figure 5 shows that each spatially varying heat transfer coefficient surface will also have a unique transient relationship.

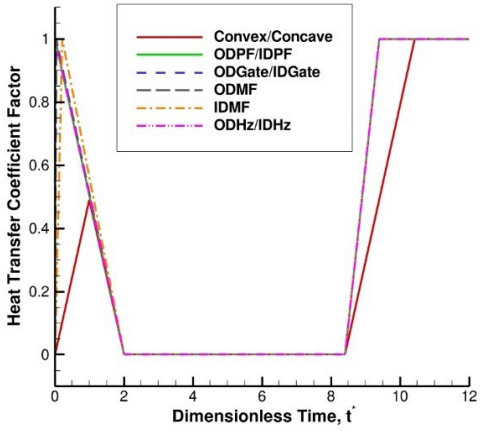

Fig. 5. Heat transfer coefficient factor as a function of dimensionless time for spatially varying heat transfer coefficient surfaces

5. THERMAL CONDITION DEFINITION FOR LOW FIDELITY MODEL

The low fidelity model had very little effort placed on defining the thermal domain of the system. The emissivity of shell and insulation wraps were taken as constant values and were the first values found through a quick and brief internet search. The emissivity of the shell was defined as a value of 0.5 by reference from [27]. The emissivity of the insulation wraps was defined as a value of 0.9 by reference from [28].

The heat transfer coefficient for the entire external mold surface was defined as a uniform relationship and had a constant value of 10 W/(m^2 · K) for atmospheric pressure casting events. Hence, the heat transfer coefficient was not unique for each individual surface of the mold. The uniform heat transfer coefficient did capture the transient behavior for pump down and vacuum break but did not consider the initial boundary layer development.

There were several other aspects not taken into consideration in terms of the thermal domain, but were considered in the nonuniform transient heat condition method, such as the transient internal mechanisms of the mold. The low fidelity model had modeled the insulation wraps with the wrap process condition. The wrap process condition only accounts for the external heat transfer mechanisms and does not take into consideration the material properties of the wrap. Therefore, by not accounting for the density and specific heat of the wraps the transient heat transfer nature of the wraps is not accurately considered. The thermal conductivity of the wraps was considered by using a thermal circuit resistance analysis to derive the total heat conductance across the external shell temperature to the ambient temperature. The total heat conductance is simply the reciprocal of the total heat resistance, Equation (12).

$$Z = R_{tot}^{(-1)} = \left(\frac{1}{h} + \frac{nb}{k}\right)^{-1} \tag{12}$$

where:

R_{tot} – total heat resistance [m^2·K/W],
n – number of insulation wraps,
b – thickness of insulation wraps [m].

The main problem with this approach is that the thermal circuit resistance analysis is only valid under steady state conditions and therefore any transient process cannot accurately be analyzed by this method. The nonuniform transient heat condition method on the other hand consisted of wraps represented by individual volumes. Which in return allowed for the assignment of a material and its thermal properties, resulting in a more accurate consideration of the thermal diffusivity.

Another aspect not considered was the radiation exchange during mold transfers. For example, the low fidelity model was modeled as always being inside of the furnace while the radiation enclosure condition had a constant emissivity and constant temperature for the entire casting process. The nonuniform transient heat condition model had a time dependent relationship for both emissivity and temperature to account for the mold transfer events. The nonuniform transient heat condition model also included the mold fixture within the furnace to account for the additional radiation mechanism while the low fidelity had no addition surfaces.

The last key difference between both modeling methodologies is with respect to the interface heat transfer coefficient between alloy and shell. The low fidelity model simply used the relationship for IN738-Mullite from the ProCAST public database and adjusted the mushy zone transition to account for the liquidus and solidus temperatures of Rene 80. The nonuniform transient heat condition model used a relationship found in the literature [2] and not only adjusted mushy zone transition temperatures but also scaled the magnitudes of IHTC to account for the differences in alloy.

There are several key significant differences between both models. The objective of comparing results of both models is to emphasize the importance in attempting to capture all the physics in the model. The scope of the current work is focused on the transient spatially varying heat transfer coefficients. The authors of the current work wished to highlight that other important aspects were not considered in either model. Examples are heat transfer at the wall between alloy and shell during filling, which will be much different than the interface heat transfer which describes the solidification process. Also, local turbulence was not considered. Finally, the IHTC between alloy and shell was only modeled as a function of temperature when we know, by findings from [3], that it also depends on geometry.

6. RESULTS AND DISCUSSION

The post processing routine for evaluating the fraction solid criteria for shrinkage porosity predictions is now presented. The fraction solid indicates the state of the alloy in the freezing range. A value of zero implies that the alloy is above the liquidus temperature, and a value of unity implies that the alloy is below the solidus temperature. An intermediate number between zero and unity implies that the alloy is in the mushy zone and dendritic growth has initiated. At some intermediate value there is a limiting fraction of solid between macro-porosity and micro-porosity. Isolated regions of fraction solid below this limit imply the micro-segregation of dendritic growth which results in shrinkage porosity. The correlation between micro-segregation and shrinkage porosity can be explained by the conservation of mass. If there is an isolated region of dendritic growth, the mass of this isolated region must remain the same. When an alloy solidifies it densifies and the only way that the density can increase is if the volume decreases. For a fixed volume in space the alloy occupying this volume must create pores to densify. Hence, the result is porosity. The limiting value of fraction solid is assumed to be 0.7 for this study.

The real-world x-ray image of the true casting is illustrated in Figure 6. The x-ray detected shrink in the upper airfoil region at approximately between mid-chord and leading-edge. The low fidelity model predictions for isolated regions of fraction solid are shown in Figure 7. After inspection of Figure 7, one can see that the model is predicting an isolated region of fraction solid in the platform airfoil fillet region. Figure 8 illustrates the total shrinkage porosity result for the low fidelity model. The indication in Figure 8 correlates with the isolated region of fraction solid in Figure 7.

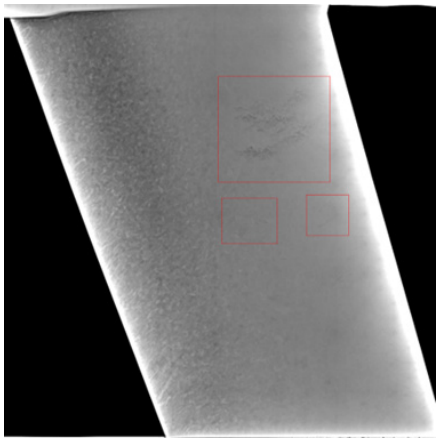

Fig. 6. Real-world x-ray image of shrink in upper airfoil region

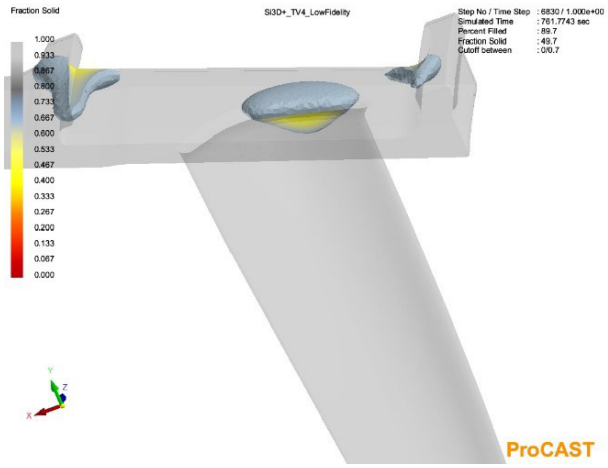

Fig. 7. Low fidelity isolated region of fraction solid model predictions

As one can conclude from evaluating both Figure 6–8, the low fidelity model does not capture the defect qualitatively. The defect is being predicted in the airfoil fillet/outer shroud region. The statistics on the defect are an average total shrinkage porosity of 21.48% and a porosity volume of 0.727 cm^3.

The predictions of isolated regions of fraction solid for the transient nonuniform model are shown in Figure 9.

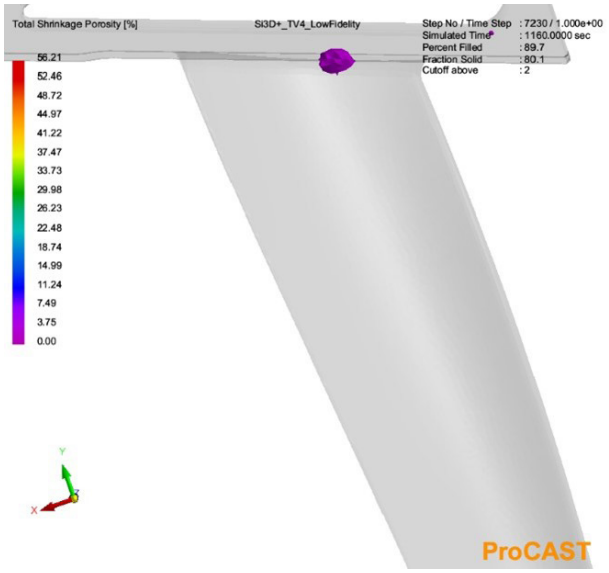

Fig. 8. Low fidelity shrinkage porosity model predictions

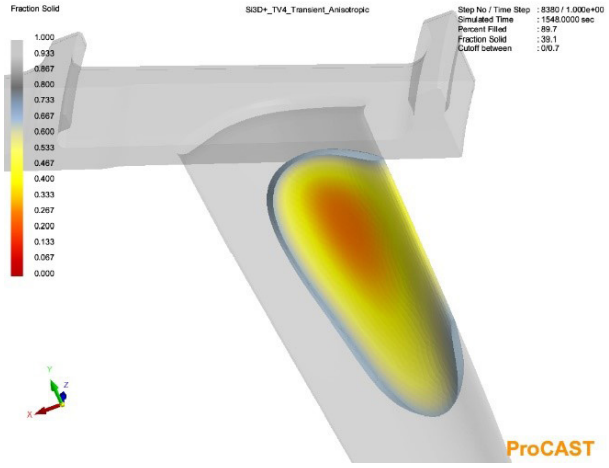

Fig. 9. Transient nonuniform isolated region of fraction solid model predictions

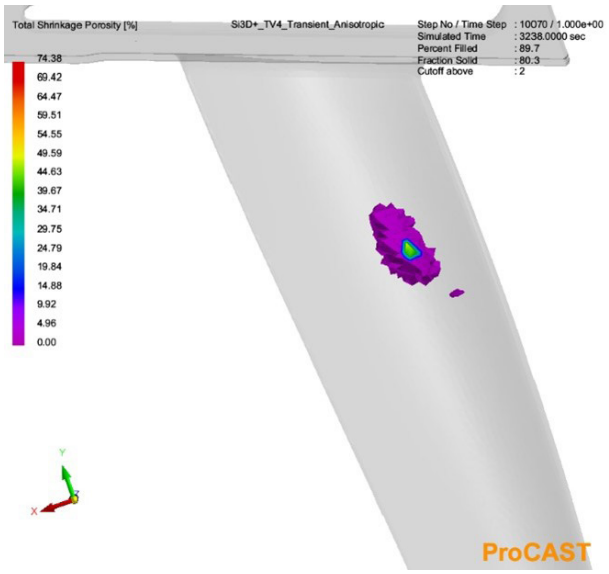

Fig. 10. Transient nonuniform shrinkage porosity model predictions

From observation of Figure 9 it is seen that the isolated region of fraction solid corresponds quite well with the indication highlighted in Figure 6. From comparing Figures 6, 9 and 10, it can be concluded that the application of the transient nonuniform methodology results in much more reliable predictions than the low fidelity methodology. The transient nonuniform model qualitatively captures the defect in relatively the same area as seen in the real-world x-ray image. The statistics on the defect are an average total shrinkage porosity of 31.65% and a porosity volume of 8.871 cm^3.

The results of both models have been presented to emphasize the importance on capturing the real-world physics in the model definition. The focus of this study was on the nonuniform natural convection heat transfer coefficients, but as mentioned in the previous section there are several other factors that also influence the overall fidelity of the model.

The statistics on the predicted defects were presented but it is recommended to evaluate the model in terms of qualitative measurements and not absolute quantities. There were still a lot of assumptions made on defining the spatially varying heat transfer coefficient conditions, but the application of the methodology was sufficient in generating reliable predictions. With reliable predictions the process modeler can iterate on process conditions, insulation schemes, and gating designs all in model space. This will result in massive amounts of savings in scrap cost and lead times associated with getting components through the product process qualifications and into production for engine set deliveries.

7. CONCLUSION

A summary of the main findings and contributions of this work are presented below:

- A thorough detailed explanation of all heat transfer mechanisms and modes is provided for each event of a general equiaxed investment casting process.
- A list of necessary assumptions needed to apply available data in the literature to the application of interest was defined.
- References to an extensive literature review with corresponding correlations used to derive the spatially varying heat transfer coefficients was given.
- Methodology for manipulating the data available in the literature for definition of the transient relationship for spatially varying heat transfer coefficient surfaces was illustrated.
- Low fidelity methodology which should not be practiced was defined and key differences between both methodologies was highlighted and explained in detail.

Due to the insufficient available research associated with the heat transfer mechanisms for equiaxed investment castings, it is planned to run a future experiment with a thermocouple mold. The expected results of the future study will provide the transient heat transfer coefficient development profile for the appropriate initial condition of the application. A continuation of the current work could also be a sensitivity study which would identify a single key aspect, of the transient nonuniform methodology, which is the main driver in

the improvements of the shrinkage porosity predictions. Other potential areas of investigation which could further enhance the fidelity of solidification process modeling predictions are as follows:

- IHTC relationships as a function of vacuum hold, alloy, and shell temperature.
- IHTC relationships between shell and insulation wraps.
- The critical fraction solid at which dendritic micro-segregation occurs and its dependence on alloy properties.
- Heat transfer between alloy and core during solidification.
- Heat transfer between alloy and shell at the wall during filling as a function of momentum and thermal boundary layers.
- Local turbulent heat transfer and its relationship to grain structure.

These are but a few of the topics which still require further investigations. The authors of this work have laid out a methodology which attempts to capture all the heat transfer mechanisms acting during the casting process. The methodology is just one of possibly many which can be used to accurately predict shrinkage porosity defects.

REFERENCES

[1] Zhang W., Xie G., & Zhang D. (2010). Application of an optimization method and experiment in inverse determination of interfacial heat transfer coefficients in the blade casting process. *Experimental Thermal and Fluid Science*, 34(8), 1068–1076. Doi: https://doi.org/10.1016/j.expthermflusci.2010.03.009.

[2] Szeliga D., Kubiak K., Ziaja W., Cygan R., Suchy J.S., Burbelko A., Nowak W.J. & Sieniawski J. (2017). Investigation of casting-ceramic shell mold interface thermal resistance during solidification process of nickel based superalloy. *Experimental Thermal and Fluid Science*, 87, 149–160. Doi: https://doi.org/10.1016/j.expthermflusci.2017.04.024.

[3] Sahai V. & Overfelt R. (1995). Contact conductance simulation for alloy 718 investment castings of various geometries. *Transactions of the American Foundrymen's Society*, 103, 627–632.

[4] Yang L., Chai L.H., Zhang L.Q. & Lin J. (2013). Numerical simulation and process optimization of investment casting of the blades for high Nb containing TiAl alloy. *Materials Science Forum*, 747–748, 105–110. Doi: https://doi.org/10.4028/www.scientific.net/MSF.747-748.105.

[5] Lenda O.B., Tara A., Jbara O., & Saad E. (2019). Numerical simulation of investment casting process of nickel-based alloy. In: *MATEC Web of Conferences*, Vol. 286, p. 03005. EDP Sciences.

[6] Miao L., Tang Z., Zhang D., Meng F., Wang J. & Li X. (2021). Investment casting simulation and analysis of shell AlSi11 alloy part. *Journal of Physics: Conference Series*, 2002(1), 012040.

[7] Liao Q., Ge P., Lu G., Yang S., Ye W., Gao J. & Luo X. (2022). Simulation study on the investment casting process of a low-cost titanium alloy gearbox based on ProCAST. *Advances in Materials Science and Engineering*, 19, 1–10. Doi: https://doi.org/10.1155/2022/4484762.

[8] Malik I., Sani A.A. & Medi A. (2020). Study on using casting simulation software for design and analysis of riser shapes in a solidifying casting component. *Journal of Physics: Conference Series*, 1500(1), 012036.

[9] Kishimoto A., Takagawa Y. & Saito T. (2020). Prevention technology of shrinkage using actual casting test and casting simulation. In: H. Okada, S.N. Atluri, *Computational and Experimental Simulations in Engineering: Proceedings of ICCES2019*. Springer International Publishing, pp. 827–837.

[10] Barot R.P. & Ayar V.S. (2020). Casting simulation and defect identification of geometry varied plates with experimental validation. *Materials Today: Proceedings*, 26(2), 2754–2762. Doi: https://doi.org/10.1016/j.matpr.2020.02.575.

[11] Kang J., Wang J., Shangguan H., Zheng L., Deng C., Hu Y. & Yi J. (2020). Modeling and simulation of the casting process with skeletal sand mold. *Materials*, 13(7), 1596. Doi: https://doi.org/10.3390/ma13071596.

[12] Domeij B., Belov I., Fourlakidis V. & Dioszegi A. (2022). Implementation and validation of casting simulation methodology for diagnostics of lamellar graphite iron. *International Journal of Metalcasting*, 17(3), 1–11. Doi: https://doi.org/10.1007/s40962-022-00892-9.

[13] Haldar P. & Sutradhar G. (2021). Simulation and validation of castings in shop floor. In: Z. Abdallah & N. Aldoumani (Eds.), *Casting Processes and Modelling of Metallic Materials*. IntechOpen, pp. 53–69, https://www.intechopen.com/chapters/74553.

[14] Hellums J.D. & Churchill S.W. (1962). Transient and steady state, free and natural convection, numerical solutions: Part I. The isothermal, vertical plate. *AIChE Journal*, 8(5), 690–692. Doi: https://doi.org/10.1002/aic.690080525.

[15] Goldstein R.J. & Briggs D.G. (1964). Transient free convection about vertical plates and circular cylinders. *ASME Journal of Heat and Mass Transfer*, 86(4), 490–500. Doi: https://doi.org/10.1115/1.3688728.

[16] Salmanpour M. & Zonouz O.N. (2008). Numerical comparison of the effect of concave and convex curvatures over the rate of heat transfer from a vertical wall in natural convection flow. *Heat Transfer Research*, 39(6), 549–558. Doi: https://doi.org/10.1615/HeatTransRes.v39.i6.90.

[17] Bhowmik H., Gharibi A., Yaarubi A. & Alawi N. (2019). Transient natural convection heat transfer analyses from a horizontal cylinder. *Case Studies in Thermal Engineering*, 14, 100422. Doi: https://doi.org/10.1016/j.csite.2019.100422.

[18] Eckert E.R.G. & Jackson T.W. (1950). *Analysis of turbulent free-convection boundary layer on flat plate* (No. NACA-TN-2207). Washington: National Advisory Committee for Aeronautics.

[19] Moran W.R. & Lloyd J.R. (1975). Natural convection mass transfer adjacent to vertical and downward-facing inclined surfaces. *ASME Journal of Heat and mass Transfer*, 97(3), 472–474. Doi: https://doi.org/10.1115/1.3450404.

[20] Vliet G.C. & Ross D.C. (1975). Turbulent natural convection on upward and downward facing inclined constant heat flux surfaces. *ASME Journal of Heat and mass Transfer,* 97(4), 549–554. Doi: https://doi.org/10.1115/1.3450427.

[21] Hrycak P. & Sandman D. . (1986). Radiative and free-convective heat transfer from a finite horizontal plate inside an enclosure. In: *14th Space Simulation Conference: Testing for a Permanent Presence in Space.* NASA Conference Publication 2446, National Aeronautics and Space Administration, pp. 42–62.

[22] Fishenden M. & Saunders O.A. (1950)., *An Introduction to Heat Transfer*. London: Oxford University Press.

[23] Bandyopadhyay K., Oosthuizen P.H. & Li Q. (2023). A numerical study of unsteady natural convection from two-sided thin horizontal isothermal plates. In: *Proceedings of the 10th International Conference on Fluid Flow, Heat and Mass Transfer (FFHMT'23)*, paper no. 108. Doi: https://doi.org/10.11159/ffhmt23.108.

[24] Yang K.T. (1987). Natural convection in enclosures. In: S. Kakac, R.K. Shah & W. Aung (Eds.), *Handbook of Single-Phase Convective Heat Transfer*. New York: John Wiley, pp. 13.1–13.51.

[25] Bauer W., Moldenhauer A. & Platzer A. (2005). Emissivities of ceramic materials for high temperature processes. *Optical Diagnostics*, 5880, pp. 263–272. SPIE. Doi: https://doi.org/10.1117/12.624512.

[26] Jones J.M., Mason P.E. & Williams A. (2019). A compilation of data on the radiant emissivity of some materials at high temperatures. *Journal of the Energy Institute*, 92(3), 523–534. Doi: https://doi.org/10.1016/j.joei.2018.04.006.

[27] Hakes S. (2011). How space shuttle technology improves crown emissivity. *Glass International*, https://www.glass-international.com/content-images/news/FIC.pdf [accessed: 22.11.2023].

[28] Unifrax LLC. (2017). Fiberfrax® Blanket and Mat Products. *Product Information Sheet*. http://buyinsulationproducts.com/files/126993874.pdf [accessed: 22.11.2023].